

# Electrochemical Detection of *Lactobacillus Rhamnosus* in Fermented Food Using Magnetic Immunosensor based on Au-Fe<sub>3</sub>O<sub>4</sub>

Yin Feng\*, Yan Liu, Ying Li, Jiamiao Lv, Haiyan Chen

School of Life Science, Changchun SCI-TECH University, Changchun 130000, China

\*E-mail: [fengyin1123@sina.com](mailto:fengyin1123@sina.com)

*Received:* 3 December 2021 / *Accepted:* 11 January 2022 / *Published:* 2 February 2022

This study was conducted on the preparation of a high stable and accurate magnetic NPs-based electrochemical immunosensor for the determination of probiotic *Lactobacillus rhamnosus* (LGG) in fermented foods. A sandwich-like immunocomplex was fabricated using Au-Fe<sub>3</sub>O<sub>4</sub> NPs, which were chemically synthesized and conjugated with a specific antibody against the pilus subunit SpaA (anti-SpaA) and a horseradish peroxidase labeled polyclonal antibody against SpaA (PcAb-HRP), and the resultant immunocomplex was used for modification of the magnetic glassy carbon electrode (PcAb-HRP/LGG/anti-SpaA/Au-Fe<sub>3</sub>O<sub>4</sub> NPs/MGCE). The structural analyses using XRD, SEM and FTIR corroborated the successful synthesis of the Au-Fe<sub>3</sub>O<sub>4</sub> NPs and immobilization of biological molecules on the surface of the Au-Fe<sub>3</sub>O<sub>4</sub> NPs. Electrochemical studies of the immunosensor using CV, DPV and EIS showed the high sensitivity, accuracy and selectivity of the developed immunosensor to determine LGG. Results revealed that the linear concentration of LGG is from 10 to 10<sup>9</sup> CFU/ml, and the limit of detection was obtained at 14 CFU/ml. The reproducibility and stability of the immunosensor were investigated, and the results indicated that the acceptable precision, stability, and repeatability of the immunosensor were related to Au NPs in PcAb-HRP/LGG/anti-SpaA/Au-Fe<sub>3</sub>O<sub>4</sub> NPs which can enhance the signal, electro-catalytic property, biocompatibility and stability of the sensor. The practical capability of the immunosensor for determination of LGG in milk and yogurt was studied and the results illustrated that the components in milk and yogurt matrices did not show any influence on immunosensor detection, implying that the developed immunosensor is a reliable electrochemical LGG sensor in food samples.

**Keywords:** Probiotic *Lactobacillus rhamnosus*; Magnetic NPs; Sandwich-like immunocomplex; Fermented food; Differential pulse voltammetry

## 1. INTRODUCTION

The probiotic strain in *Lactobacillus rhamnosus* GG (LGG) is a bacteria that exists naturally in the body, primarily in the intestines [1]. LGG has been used as a probiotic, or friendly bacteria, to

prevent the growth of harmful bacteria in the stomach and intestines, and has been used in alternative medicine as a likely effective aid in treating or preventing diarrhea caused by rotavirus in babies and children. It has also been used to treat Crohn's disease, lactose intolerance, and vaginal yeast infections [2, 3].

*L. rhamnosus* is sometimes used as a dietary supplement, added to a variety of foods, and used in fermented dairy products [4-6]. LGG is a good starter for fermentation of dairy and can be added to dairy products such as yogurts and milk to boost their probiotic content and to cheeses to aid the ripening process [7, 8]. The health-beneficial effects of these bacteria depend on their adhesion capacity and residence time in the gastrointestinal tract [9, 10]. The bacterial count is an important factor in fermentation of dairy products and has an influence on fermentation and expiration time [11].

Therefore, determination of the LGG is necessary for its application in dietary supplements and fermentation of dairy products [12, 13]. However, the determination of *L. rhamnosus* is difficult and laborious, and is based on its physiological and biochemical properties [14]. Accordingly, a few studies have been carried out using PCR, chromatography-mass spectrometry and electrochemical techniques for identification and determination of *L. rhamnosus* in fermented food samples [15-19]. Among these studies, electrochemical immunomagnetic NPs based sensors show good selectivity and sensitivity [15-17]. However, these sensors do not show sufficient stability and repeatability and they need more investigation. Therefore, this study was conducted on the preparation of the highly stable and accurate magnetic NPs-based electrochemical immunosensor for the determination of probiotic *Lactobacillus rhamnosus* in fermented foods.

## 2. EXPERIMENTAL

### 2.1. Strains *L. rhamnosus* GG and culture conditions

Strains *L. rhamnosus* Goldin and Gorbach (LGG, Shandong Pingao Pharmaceutical Co. Ltd., China) were anaerobically grown in The de Man, Rogosa and Sharpe (MRS, Merckmillipore, Germany) medium at 36 °C for 24 hours. For collection of the bacterial cells, the bacterial suspension was centrifuged at 4500 g for 8 minutes. Subsequently, the cells were suspended in 10mM of phosphate-buffered saline (PBS, Sigma-Aldrich) (pH 7.4), and adjusted to the desired optical density (Lambda 20 Spectrophotometer, Shimadzu, Tokyo, Japan) of 0.5 at 600 nm (OD<sub>600</sub>). For assessment of the exact concentration of bacteria suspension, suitable dilutions of the bacterial suspensions were plated onto MRS agars [20].

### 2.2. Preparation of antibody coated magnetic nanoparticles (*anti-SpaA*- Au- $Fe_3O_4$ NPs)

$Fe_3O_4$  nanoparticles were synthesized by mixture containing 2 g of  $Fe(C_5H_7O_2)_3$  (97%, Sigma-Aldrich), 2.6 g of 1, 2-hexadecanediol (90%, Merck, Germany), 2 ml of oleic acid (), 20 ml of phenyl ether (98%, Jinan Realong Chemical Co., Ltd., China) and 20 ml of oleylamine (70%, Sigma-Aldrich) [21]. The mixture was stirred for 1 hour to obtain a bright red suspension, and then transferred into a

flask and heated to 210 °C. After 2 hours, the flask was cooled and the resultant Fe<sub>3</sub>O<sub>4</sub> NPs in a dark brown color were obtained.

To prepare the Au-Fe<sub>3</sub>O<sub>4</sub> NPs, the result was 1 g of Fe<sub>3</sub>O<sub>4</sub> NPs dispersed in 20 phenyl ether. Then, the mixture of 0.9 g of HAuCl<sub>4</sub>·3H<sub>2</sub>O (99%, Sigma-Aldrich), 1g of polyvinyl alcohol (PVA, 99.9%, Qingdao Shida Chemical Co., Ltd., China), 3 g of 1,2-hexadecanediol, 2 mL of oleylamine and 0.5 mL of oleic acid were stirred and added to dispersed Fe<sub>3</sub>O<sub>4</sub> NPs suspension. The resultant suspension was heated to 185°C for 15 minutes, and maintained at this temperature for 120 minutes. After cooling, 5 mL of the suspension was mixed with 15 mL of ethanol (99%, Dongying City Longxing Chemical Co., Ltd., China, and the mixture were stirred to obtain a dark blue suspension. Subsequently, the NPs were separated from the aqueous solution by a magnet. The separated NPs were washed several times with 10 mL of ethanol, and dispersed in 10 mL of hexanes (95%, Sigma-Aldrich) to obtain dark red-purple suspension. The suspension glass was covered by foil and stored in the refrigerator for future use.

In order to prepare antibody coated magnetic based NPs (anti-SpaA/Au-Fe<sub>3</sub>O<sub>4</sub> NPs), the prepared Au-Fe<sub>3</sub>O<sub>4</sub> NPs were washed with 500 μl of 10 mM Morpholinoethanesulfonic Acid buffer (MEST, 99.5%, Sigma-Aldrich) pH 6.0. Afterwards, Au-Fe<sub>3</sub>O<sub>4</sub> NPs were suspended in 500 μl of mixture of 20 g/l 1-ethyl-3-(3-dimethylaminopropyl) carbodiimide hydrochloride (EDC, 98%, Sigma-Aldrich), 20 g/l N-hydroxysuccinimide sodium salt (NHSS, ≥99%, Sigma-Aldrich) and 10 mM MEST buffer at 36°C. After 3 hours, the Au-Fe<sub>3</sub>O<sub>4</sub> NPs were collected and suspended with 500 μl of 10mM PBS with 0.1% Tween 20 (PBST) pH 7.4. Then, polyclonal antibodies (PcAb) against the recombinant specific antibody against the pilus subunit (SpaA) of *L. rhamnosus* GG (PcAb-SpaA) were added into the suspension and incubated for 2 hours at 37 °C. After that, anti-SpaA/Au-Fe<sub>3</sub>O<sub>4</sub> NPs were prepared by adding the anti-SpaA solution, and incubation for 2 hours at 37°C for 2 hours. After that, the antibody coated substrate was blocked with 5% (w/v) bovine serum albumin (BSA, 99%, Merck, Germany) for 60 minutes at 37° C [22]. Next, the substrate was rinsed three times with PBST. Following a PBST wash, anti-SpaA/Au- Fe<sub>3</sub>O<sub>4</sub> NPs were suspended in a medium containing 10 g/l PBST, 5% BSA and 0.05% NaN<sub>3</sub> (99%, Merck, Germany).

### 2.3. Characterization of anti-SpaA/Au-Fe<sub>3</sub>O<sub>4</sub> NPs

For analysis of the molecular structure of the nanoparticles with attenuated total reflectance-Fourier transform infrared (ATR-FTIR; Bruker Hyperion 3000 Microscope with a Vertex 70 Bench and HTS Plate Reader), 10 μg of Au-Fe<sub>3</sub>O<sub>4</sub> NPs and anti-SpaA-Au- Fe<sub>3</sub>O<sub>4</sub> NPs were separately dried, and evenly mixed with 0.2 g of KBr (≥99%, Sigma-Aldrich) and pressed into thin sheets to prepare the transparent disc. Transmission electron microscopy (TEM; JEOL 1200EX TEMSCAN) and scanning electron microscopy (SEM; S4800, Hitachi, Tokyo, Japan) were applied for analysis of the morphology the NPs. For TEM analysis, NPs suspensions were diluted to 600 g/l in milliQ water, and drop cast onto the TEM grid. Crystalline studies were carried out using X-ray diffraction (XRD, PANalytical Empyrean Series 2).

## 2.4. Electrochemical studies

All electrochemical studies were carried out according to [15, 16, 23], and performed using cyclic voltammetry (CV), differential pulse voltammetry (DPV) and electrochemical impedance spectroscopy (EIS) which were conducted on the electrochemical workstation (Autolab, Eco Chemie, The Netherlands) using magnetic glassy carbon electrode (MGCE) as the working electrode, Pt wire as the counter electrode, and saturated calomel electrode (SCE) as the reference electrode. The electrochemical cell was contained 10mM PBS (pH 7.4) containing 0.1 M KCl (99%, Jiangsu Xfnano Materials Tech Co.,China) and 5 mM of  $\text{Fe}(\text{CN})_6^{3-/4-}$  ( $\geq 99\%$ , Sigma-Aldrich), and 10mM PBS (pH 7.4) containing 1.0 mM  $\text{H}_2\text{O}_2$  (30 % (w/w), Sigma-Aldrich) and 1.0 mM hydroquinone (HQ,  $\geq 99\%$ , Sigma-Aldrich) as electrolytes. EIS measurements were performed at a frequency range from  $10^{-1}$  Hz to  $10^5$  Hz with an applied 5 mV sine wave ac voltages. For modification of the MGCE, A sandwich immunoassay strategy was used as illustrated in Figure 1, according to the reported strategy to detect probiotic strains [16, 24]. For electrochemical analyses, 1 mL of LGG suspension ( $\sim 10^5$  CFU/ml) was gently mixed with 10  $\mu\text{g}$  of PcAb-SpaA/Au- $\text{Fe}_3\text{O}_4$  NPs, transferred into centrifuge tubes, and mixed with 10  $\mu\text{L}$  of fluorescein isothiocyanate (FITC,  $\geq 97.5\%$ , Sigma-Aldrich) conjugated with 2 g/l goat anti-rabbit IgG (type M-280 Dynabeads, Dynal UK Ltd., Wirral, United Kingdom), and suspended in 0.2 mL of 10mM PBS (pH 7.4). The tube was incubated for 1 hour at 37 °C on a Dynal sample mixer. After immunocapture, the complex of immunomagnetic NPs and bacteria (IMNPs-bacteria) was separated by applying an external magnetic force for 3 minutes, washed with 0.5 ml PBST several times, and then suspended in 0.2 ml of 10mM PBS (pH 7.4). To link the bacteria cell suspension, 10 l of 2.5 g/l horseradish peroxidase (HRP; Nanjing Duly Biotech Co., Ltd., China) labeled polyclonal antibody against SpaA (PcAb-HRP) was added and incubated for 1 hour at 37°C (PcAb-HRP/LGG/IMNPs-bacteria). It was followed by the collection of the obtained IMNPs- bacteria complex using the external magnet, and washing the complex using 0.5 ml PBST. The complex was resuspended in 10mM PBS (pH 7.4) and used for modification of the working electrode through the immersion of the MGCE in final suspension of complex for 20 minutes.

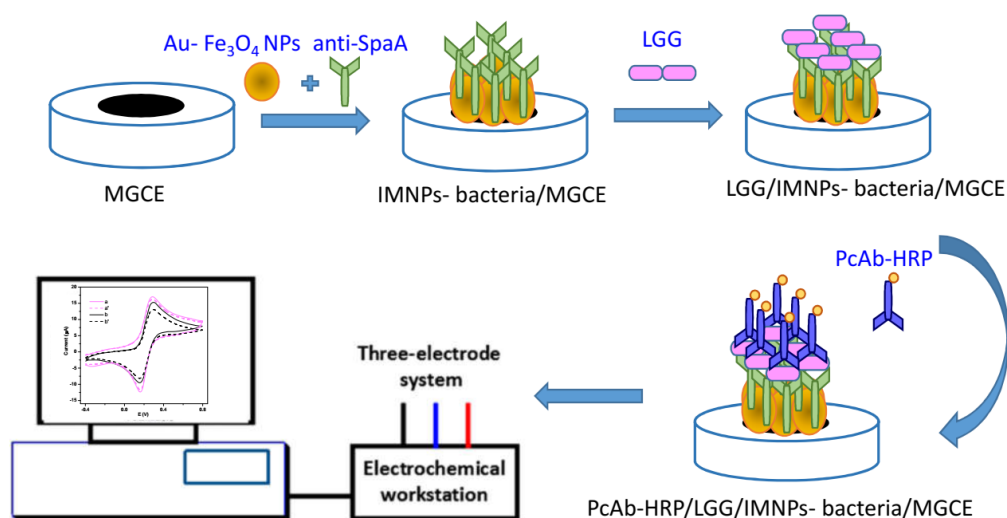


**Figure 1.** Schematic Illustration of the modification electrode and electrochemical detection process

For electrochemical detection measurements, the spiked samples were prepared as follows: A prepared LGG suspension containing  $10^9$  CFU/ml was diluted tenfold in 10mM PBS (pH 7.4). As a control sample, 1ml of bacterial suspension and 10mM PBS (pH 7.4) were placed in a microcentrifuge tube. After 10 $\mu$ l of magnetic based NPs were added to tubes for incubation and immunocapturing, the tubes were transferred to a Dynal sample mixer for 1 hour at 37 °C. It was followed by separation of IMNPs- bacteria complex via external magnet force, washing the complex using 0.5 ml PBST for several times, and suspending the complex in 0.5 ml of 10mM PBS (pH 7.4). Following that, 10  $\mu$ l of 2.5 g/l PcAb-HRP was added to the resultant bacterial suspension (IMNPs-bacteria-PcAb-HRP complex), and then incubated for 1 hour at 37 °C. So, the final complex was collected via external magnet force, washed with 0.5 ml of PBST several times, and suspended in 0.1 ml of 10mM PBS (pH 7.4). Then, MGCE was immersed in the final complex for 20 minutes, subsequently washed and stored in the refrigerator for future electrochemical experiments.

For characterization of the magnetic NPs-based electrochemical immunosensor, 1 ml of LGG suspension along with several lactic acid bacteria species (Shandong Zhongke-Jiayi Bioengineering Co., Ltd., China) including *L. casei* BL23 (BL23), *L. bulgaricus* Lbb03 (Lbb03), *L. plantarum* Lp3 (Lp3), *L. fermentum* Lf09 (Lf09), *Enterococcus faecium* M0 (M0), *L. paracasei* Fg02 (Fg02), *Streptococcus thermophilus* St05 (St05) and *Pediococcus pentosaceus* H13 (H13), and anaerobic bacteria from rat (RTT) and human (HFF) feces (Zhengzhou Zikun Environmental Protection Technology Co., Ltd., China) were used to study the selectivity of proposed immunosensor.

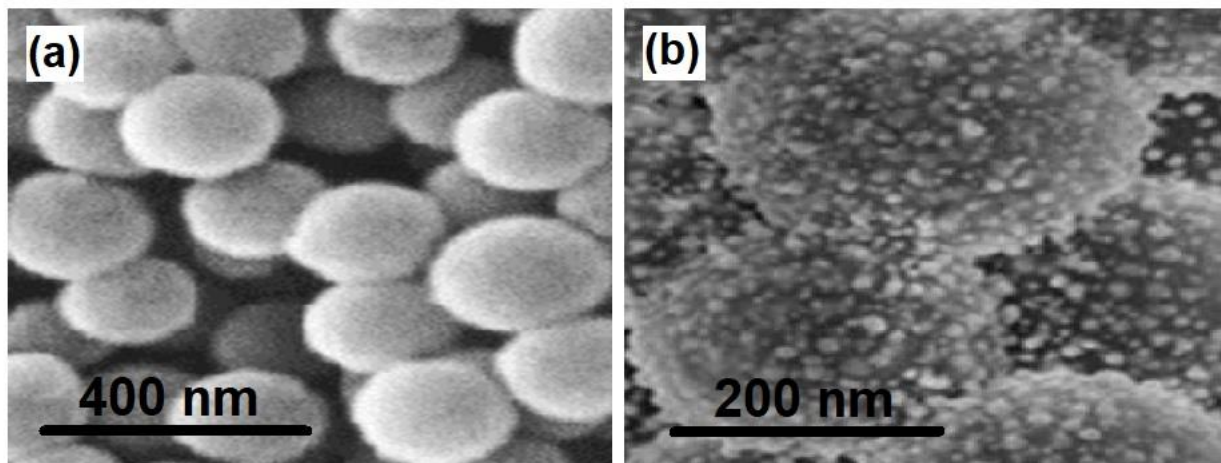
### 2.5. Study the real food sample

To evaluate the applicability of the IMNPs in the determination of LGG in complex food matrices, the samples of milk and commercial yogurt (I and II samples referred to without and with label LGG, respectively) were provided. The food samples were spiked with LGG and utilized to study the proposed immunosensor performance. For electrochemical measurements, one milliliter of samples was diluted 100 times in 10mM PBS (pH 7.4). The concentration of lactic acid bacteria was determined by plating serial dilutions on MRS agar.

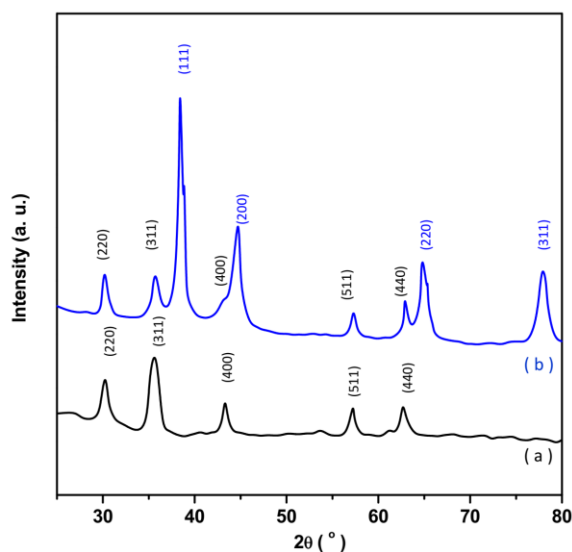
## 3. RESULTS AND DISCUSSION

### 3.1. Structural studies of prepared nanocomposite

Figure 2 shows the SEM images of Fe<sub>3</sub>O<sub>4</sub> NPs and Au-Fe<sub>3</sub>O<sub>4</sub> NPs. The SEM image in Figure 2a shows that Fe<sub>3</sub>O<sub>4</sub> NPs were synthesized in a sphere-shape with an average diameter of ~ 200nm. Figure 2b shows a substantial number of Au particles with a smaller average size (~20nm) are evenly distributed on the Fe<sub>3</sub>O<sub>4</sub> NPs surface to form a magnetic based composite of Au-Fe<sub>3</sub>O<sub>4</sub> NPs. These observations indicate that Au NPs were successfully decorated on the surface of Fe<sub>3</sub>O<sub>4</sub> NPs. Moreover, it is notable that the decoration of Au NPs on Fe<sub>3</sub>O<sub>4</sub> NPs does not change their morphology.

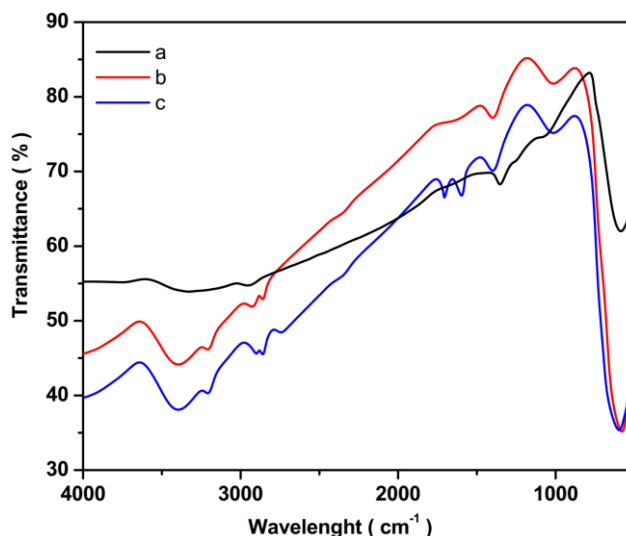


**Figure 2.** SEM images of (a)  $\text{Fe}_3\text{O}_4$  NPs and (b)  $\text{Au-Fe}_3\text{O}_4$  NPs



**Figure 3.** Results of the XRD analysis of (a)  $\text{Fe}_3\text{O}_4$  NPs and (b)  $\text{Au-Fe}_3\text{O}_4$  NPs

Figure 3 shows the results of the XRD analysis of  $\text{Fe}_3\text{O}_4$  NPs and  $\text{Au-Fe}_3\text{O}_4$  NPs. As observed from Figure 3, XRD pattern of  $\text{Fe}_3\text{O}_4$  NPs displays the diffraction peaks at  $2\theta = 30.13^\circ$ ,  $35.57^\circ$ ,  $43.38^\circ$ ,  $57.02^\circ$  and  $62.70^\circ$ , which are related to the (220), (311), (400), (511), and (440) planes, respectively, which are in good accordance with the inverse cubic spinel phase of  $\text{Fe}_3\text{O}_4$  (JCPDS card no.00-85-1436) [25]. It can be observed from Figure 3b that the XRD pattern of  $\text{Au-Fe}_3\text{O}_4$  NPs shows the same peaks of  $\text{Fe}_3\text{O}_4$  and additional diffraction peaks at  $2\theta = 38.20^\circ$ ,  $44.541^\circ$ ,  $64.69^\circ$  and  $77.70^\circ$  that these can be assigned to (111), (200), (220), and (311) planes of face-centered cubic (fcc) Au NPs (JCPDS card no. 04-0784), respectively, which decorated the  $\text{Fe}_3\text{O}_4$  NPs [26]. Therefore, the XRD, SEM and TEM data corroborate the successful synthesis of the  $\text{Au-Fe}_3\text{O}_4$  NPs.



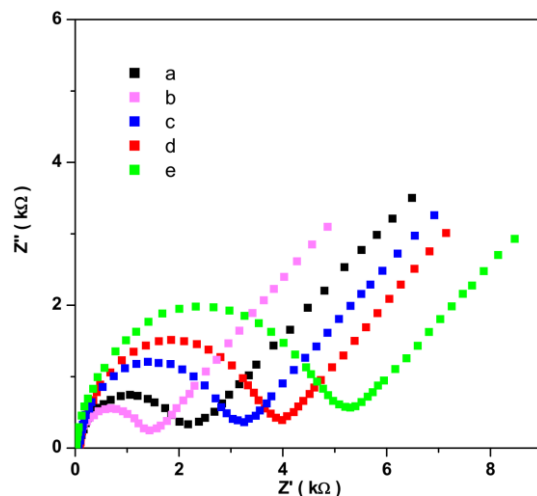
**Figure 4.** FTIR spectrum of (a)  $\text{Fe}_3\text{O}_4$  NPs, (b)  $\text{Au-Fe}_3\text{O}_4$  NPs and (c) anti-SpaA/ $\text{Au-Fe}_3\text{O}_4$  NPs.

Figure 4 also exhibits the FTIR spectrum of  $\text{Fe}_3\text{O}_4$  NPs,  $\text{Au-Fe}_3\text{O}_4$  NPs and anti-SpaA/ $\text{Au-Fe}_3\text{O}_4$  NPs. As seen from the FTIR spectrum of  $\text{Au-Fe}_3\text{O}_4$  NPs, there is a peak at  $3379\text{ cm}^{-1}$  that it is related to O–H stretching vibrations which originate from -OH groups in phenyl ether and water adsorbed on the  $\text{Au-Fe}_3\text{O}_4$  NPs [27]. The absorption band is observed at  $2898\text{ cm}^{-1}$  which is assigned to adsorbed oleate species of oleic acid [28]. The Fe-O vibrations are shown to have peaks at  $1379$  and  $564\text{ cm}^{-1}$  [29]. The FTIR spectrum of  $\text{Au-Fe}_3\text{O}_4$  NPs contains all the peaks of the FTIR spectrum of  $\text{Fe}_3\text{O}_4$ , and two additional peaks vibrations of C=O groups and O-H groups of PVA at  $2914\text{ cm}^{-1}$  and  $3318\text{ cm}^{-1}$  [26], respectively, indicating the successful synthesis of the  $\text{Au-Fe}_3\text{O}_4$  NPs nanocomposite. The FTIR spectrum of anti-SpaA/ $\text{Au-Fe}_3\text{O}_4$  NPs contains all the peaks from the FTIR spectra of  $\text{Au-Fe}_3\text{O}_4$  NPs, and additional peaks at  $1692\text{--}1635\text{ cm}^{-1}$ , which are attributed to the formation of an amide bond from the antibody [30, 31], demonstrating to anti-SpaA particles were successfully immobilized on the surface of  $\text{Au-Fe}_3\text{O}_4$  NPs.

### 3.2. Electrochemical studies of the immunosensor

The EIS analysis of the bare and modified MGCE in 10mM PBS (pH 7.4) containing 0.1 M KCl and 5mM  $\text{Fe}(\text{CN})_6^{3-/4-}$  is shown in Figure 5. The charge transfer resistance ( $R_{ct}$ ) values can be directly obtained from the semicircle radius in the Nyquist plots [32, 33]. A comparison between the obtained Nyquist plots shows that after the modification MGCE surface by  $\text{Au-Fe}_3\text{O}_4$  NPs, the impedance value is decreased because of the higher conductivity of the Au NPs that decorated the  $\text{Fe}_3\text{O}_4$  NPs surface. Moreover, it is observed that  $R_{ct}$  value increased continuously with modification of MGCE surface by anti-SpaA/ $\text{Au-Fe}_3\text{O}_4$  NPs (Figure 5c), LGG/anti-SpaA/ $\text{Au-Fe}_3\text{O}_4$  NPs (Figure 5d) and PcAb-HRP/LGG/anti-SpaA/ $\text{Au-Fe}_3\text{O}_4$  NPs (Figure 5e) which illustrated to the successful functionalization of the  $\text{Au-Fe}_3\text{O}_4$  NPs/MGCE by anti-SpaA, LGG/anti-SpaA and PcAb-HRP/LGG/anti-SpaA [34], respectively, and longer electron transfer path, and the large resistance of

biomolecules, subsequently prevents electron transfer [35]. These observations demonstrate that PcAb-HRP, LGG and anti-SpaA as biomolecules bind to the surface of Au-Fe<sub>3</sub>O<sub>4</sub> NPs and could hinder the electron transfer by formation of an insulating film [36].



**Figure 5.** EIS analysis of the (a) bare MGCE, and (b) Au-Fe<sub>3</sub>O<sub>4</sub> NPs, (c) anti-SpaA/Au-Fe<sub>3</sub>O<sub>4</sub> NPs, (d) LGG/anti-SpaA/Au-Fe<sub>3</sub>O<sub>4</sub> NPs and (e) PcAb-HRP/LGG/anti-SpaA/Au-Fe<sub>3</sub>O<sub>4</sub> NPs modified MGCE in 10 mM PBS (pH7.4) containing 0.1M KCl and 5mM of Fe(CN)<sub>6</sub><sup>3-/4-</sup>.

Further electrochemical analyses were carried out using the CV measurements in bare and modified MGCE in 10mM PBS (pH7.4) containing 0.1M KCl and 5 mM of Fe(CN)<sub>6</sub><sup>3-/4-</sup> at scan rate of 50mV/s. Figure 6 shows that all electrodes exhibit a reversible CV, and with a peak-to-peak separation ( $\Delta E_p$ ) of 0.12, 0.11, 0.21, 0.30 and 0.31V for bare MGCE, and Au-Fe<sub>3</sub>O<sub>4</sub> NPs, anti-SpaA/Au-Fe<sub>3</sub>O<sub>4</sub> NPs, LGG/anti-SpaA/Au-Fe<sub>3</sub>O<sub>4</sub> NPs and PcAb-HRP/LGG/anti-SpaA/Au-Fe<sub>3</sub>O<sub>4</sub> NPs modified MGCE, respectively. The peak current is also increased after modification the MGCE by Au-Fe<sub>3</sub>O<sub>4</sub> NPs. The increase in current and decrease  $\Delta E_p$  Au-Fe<sub>3</sub>O<sub>4</sub> NPs/MGCE can be related to the synergistic effect of nano-sized and conductive metal particles in the fabrication of Au-Fe<sub>3</sub>O<sub>4</sub> NPs nanocomposite [37, 38]. However, peak current value are increased and  $\Delta E_p$  are decreased for anti-SpaA/Au-Fe<sub>3</sub>O<sub>4</sub> NPs, LGG/anti-SpaA/Au-Fe<sub>3</sub>O<sub>4</sub> NPs and PcAb-HRP/LGG/anti-SpaA/Au-Fe<sub>3</sub>O<sub>4</sub> NPs modified MGCE, indicating immobilization of the biological macromolecules on the electrode surface restrict the effective area and active sites necessary for electron transfer, block the diffusion of electrolyte ions towards the electrode surface [37]. In addition, it is observed that the peak current of PcAb-HRP/LGG/anti-SpaA/Au-Fe<sub>3</sub>O<sub>4</sub> NPs is higher than that of LGG/anti-SpaA/Au-Fe<sub>3</sub>O<sub>4</sub> NPs modified MGCE, because HRP acts as an enzyme label for amplification of electrochemical signals [39, 40].

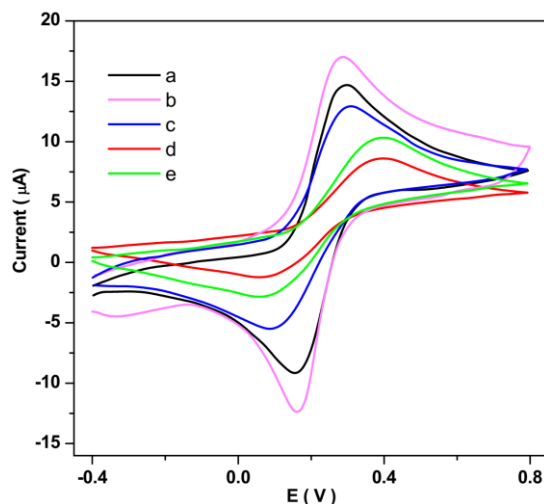


**Figure 6.** CV curves of the (a) bare MGCE, and (b) Au-Fe<sub>3</sub>O<sub>4</sub> NPs, (c) anti-SpaA/Au-Fe<sub>3</sub>O<sub>4</sub> NPs, (d) LGG/anti-SpaA/Au-Fe<sub>3</sub>O<sub>4</sub> NPs and (e) PcAb-HRP/LGG/anti-SpaA/Au-Fe<sub>3</sub>O<sub>4</sub> NPs modified MGCE in 10mM PBS (pH 7.4) containing 0.1M KCl and 5mM of Fe(CN)<sub>6</sub><sup>3-/4-</sup> at scan rate of 50mV/s.

In order to study the Au NPs in electrochemical activity, the stability of electrochemical response of PcAb-HRP/LGG/anti-SpaA/Au-Fe<sub>3</sub>O<sub>4</sub> NPs/MGCE and PcAb-HRP/LGG/anti-SpaA/Fe<sub>3</sub>O<sub>4</sub> NPs/MGCE was studied in 10mM PBS (pH7.4) containing 0.1M KCl and 5mM of Fe(CN)<sub>6</sub><sup>3-/4-</sup> at scan rate of 50mV/s.

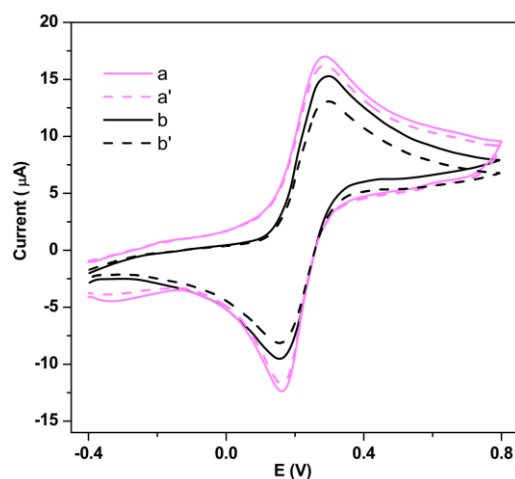


**Figure 7.** CV curves of first (solid line) and 100<sup>th</sup> (dashed line) sweeps of (a and a') PcAb-HRP/LGG/anti-SpaA/Au-Fe<sub>3</sub>O<sub>4</sub> NPs and (b and b') PcAb-HRP/LGG/anti-SpaA/Fe<sub>3</sub>O<sub>4</sub> NPs modified MGCE in 10 mM PBS (pH7.4) containing 0.1M KCl and 5mM of Fe(CN)<sub>6</sub><sup>3-/4-</sup> at scan rate of 50mV/s.

Figure 7 shows the initial CV curve and the obtained CV curve after successive 100 sweeps which indicated a 3.6% and 13.5% change for the electrochemical current of PcAb-HRP/LGG/anti-

SpaA/Au-Fe<sub>3</sub>O<sub>4</sub> NPs and PcAb-HRP/LGG/anti-SpaA/ Fe<sub>3</sub>O<sub>4</sub> NPs modified MGCE, respectively. Furthermore, the current peak of PcAb-HRP/LGG/anti-SpaA/Au-Fe<sub>3</sub>O<sub>4</sub> NPs is higher than that of PcAb-HRP/LGG/anti-SpaA/ Fe<sub>3</sub>O<sub>4</sub> NPs, implying to the employed Au NPs as assisting matrices causes that signal enhancement, promote electro-catalytic property, excellent electron movement ability and favorable biocompatibility with antibody or antigen [41, 42]. Thus, the results of EIS and CV analyses confirm the perfect biocompatibility of the obtained immunosensor and the capturing ability for LGG, and the following electrochemical studies were conducted on the PcAb-HRP/LGG/anti-SpaA/Au-Fe<sub>3</sub>O<sub>4</sub> NPs/MGCE immunosensor.

To study the electrochemical determination of *L. rhamnosus* GG, DPV measurements were performed in 10mM PBS (pH 7.4) containing 1.0 mM H<sub>2</sub>O<sub>2</sub> and 1.0 mM HQ for successive spike of bacterial suspensions at a scan rate of 50mV/s. To prepare the artificial medium, the bacterial suspensions included different concentrations of LGG and *Lactobacillus casei* BL23 as control. Figure 8 shows DPV curves as electrochemical response to different concentrations of LGG and resulted calibration plot of immunosensor. It is observed that the peak current increases with the increase in LGG concentration because of the catalytic reaction of HRP in H<sub>2</sub>O<sub>2</sub>-HQ system [39, 43]. The calibration plot reveals that the linear of LGG concentration is from 10 to 10<sup>9</sup> CFU/ml, and the limit of detection is obtained at 14 CFU/ml. The lower value of limit of detection can minimize the complexity and diversity of relevant food matrices [44]. In addition, the peak current of DPV shows no changes with the increase of *Lactobacillus casei* BL23 during the measurements, implying that the proposed immunosensor exhibits the specific performance for LGG. Table 1 presents the comparison between obtained sensing values of developed immunosensor in this study and other reported LGG sensors. It is indicated that the obtained sensing values in this study are acceptable and suggest Au NPs in PcAb-HRP/LGG/anti-SpaA/Au-Fe<sub>3</sub>O<sub>4</sub> NPs can enhance the signal, electro-catalytic property, biocompatibility and stability of the sensor [41, 42].

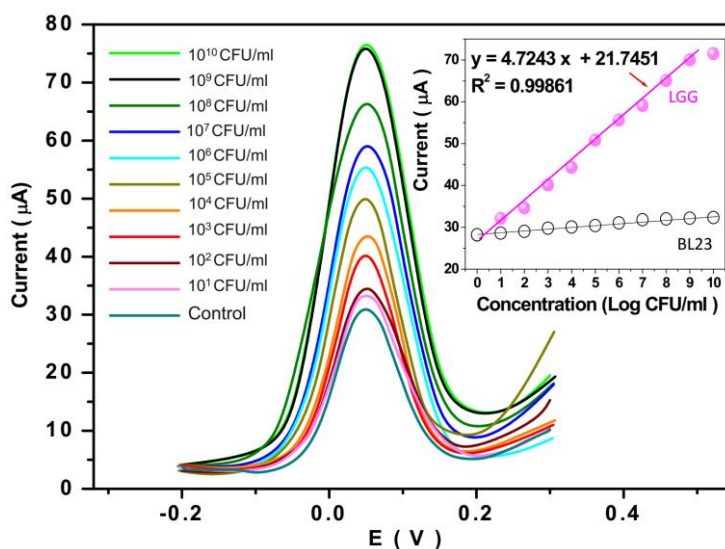


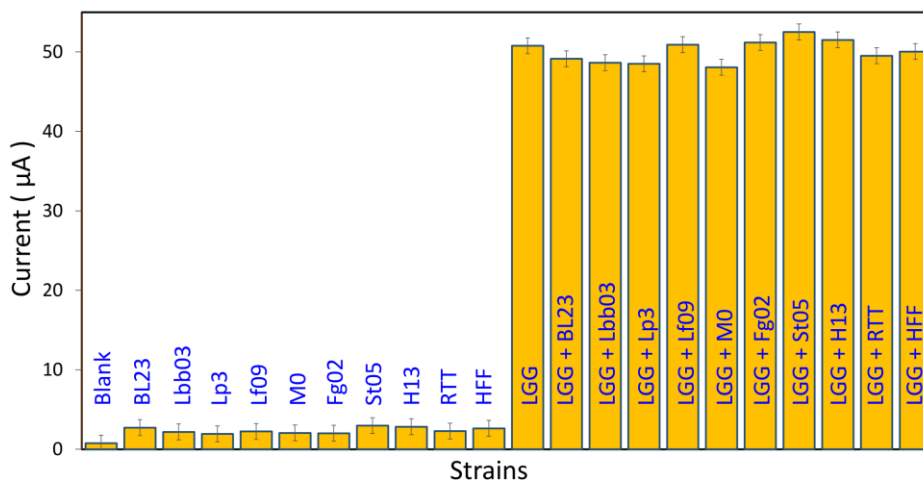
**Figure 8.** DPV measurements and obtained calibration plot of PcAb-HRP/LGG/anti-SpaA/Au-Fe<sub>3</sub>O<sub>4</sub> NPs modified MGCE in 10mM PBS (pH7.4) containing 1.0mM H<sub>2</sub>O<sub>2</sub> and 1.0mM HQ for successive spike of bacterial suspensions at scan rate of 50mV/s.

**Table 1.** Comparison between obtained sensing values of developed immunosensor in this study and other reported LGG sensors.

Sensor	Technique	Linear range (CFU/ml)	Limit of detection (CFU/ml)	Ref.
Immunosensor	DPV	10 to 10 <sup>9</sup>	14	This work
Magnetic bead-based immunosensor	DPV	2560 to 2.56 × 10 <sup>7</sup>	22	[16]
Anti-spaa/Magnetic nanobeads	IMS-CIB	29 to 2.4 × 10 <sup>6</sup>	29	[15]
N/O/hierarchical porous graphitic carbon	DPV	-	2	[17]
DH-GC-MS/8O	DH-GC-MS/8O	-	10	[18]

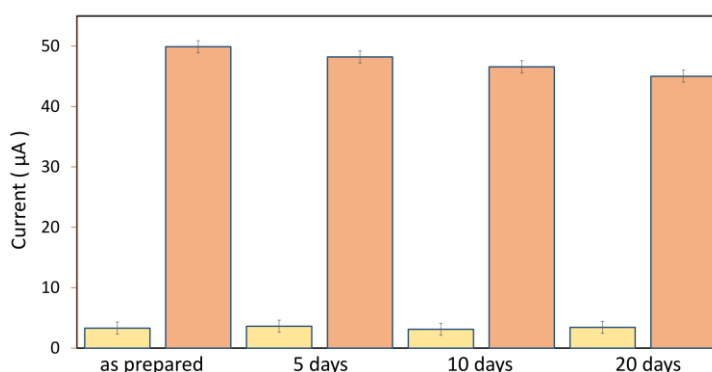
IMS-CIB: immunomagnetic separation with colony immunoblotting; DH-GC-MS/8O: eight-way olfactometry coupled to gas chromatography-mass spectrometry

Figure 9 shows the results of the study on the selectivity of the proposed immunosensor to determination of 10<sup>5</sup> CFU/ml bacterial suspensions from LGG in present 10<sup>5</sup> CFU/ml of interferents using the DPV measurements in 10mM PBS (pH7.4) containing 1.0mM H<sub>2</sub>O<sub>2</sub> and 1.0mM HQ at a scan rate of 50mV/s. The interferents included several lactic acid bacteria species (BL23, Lbb03, Lp3, Lf09, M0, Fg02, St05 and H13 strains) and anaerobic bacteria (RTT and HFF feces). It can be observed that the signal current exhibits the no remarkable differences after addition interferents, and the signal current presents the considerable increase after addition LGG and mixtures of LGG and interferents. These observations confirm that the proposed immunosensor has great specificity due to the selectivity to determination of bacterial suspensions from LGG. Use of appropriate antibody is important step in designing the immunosensor of probiotic *L. rhamnosus*. In this study, Ab-SpaA was used as antibody pilus subunit of *L. rhamnosus* GG that the pili on the cell surface of *Lactobacillus rhamnosus* GG are recognized to be key molecules for binding to human intestinal mucus which mediates the direct interaction with the host and abiotic surfaces, and also causes anti-inflammatory effects [45]. The resulting sandwich-like immunocomplex of PcAb-HRP/LGG/IMNPs-bacteria can be magnetically attached to the work's surface as a substrate for an electrochemical transducer (Figure 1). All of immunoreactions take place on the immunocomplex, and the biorecognition event can be evaluated by the electrochemically measurement and change of signal current generated in the presence of the HQ/H<sub>2</sub>O<sub>2</sub> where HQ can be catalytically oxidized to para-benzoquinone (BQ) in the presence of H<sub>2</sub>O<sub>2</sub> [46-48]. Thereupon, a reduction current of BQ is formed in the HRP-catalyzed enzymatic reaction. The changes in current signal are associated with the presence and number of LGG in the sample in the electrochemical cell.



**Figure 9.** The results study the selectivity of PcAb-HRP/LGG/anti-SpaA/Au-Fe<sub>3</sub>O<sub>4</sub> NPs/MGCE to determination of 10<sup>5</sup> CFU/ml bacterial suspensions from LGG in present 10<sup>5</sup> CFU/ml of interferents using the DPV measurements in 10mM PBS (pH 7.4) containing 1.0mM H<sub>2</sub>O<sub>2</sub> and 1.0mM HQ at scan rate of 50mV/s.

For studying the reproducibility of the proposed immunosensor, two series of four different electrodes of PcAb-HRP/LGG/anti-SpaA/Au-Fe<sub>3</sub>O<sub>4</sub> NPs/MGCE were synthesized, and used for the determination of 10<sup>5</sup> CFU/ml bacterial suspensions from LGG through the DPV technique in 10mM PBS (pH7.4) containing 1.0mM H<sub>2</sub>O<sub>2</sub> and 1.0 mM HQ at a scan rate of 50mV/s. Figure 10 shows the results of the study on the reproducibility of proposed immunosensor which indicated that the relative standard deviation (RSD) values of the four immunosensors were obtained with less than 3.82%, implying an acceptable precision and repeatability of the immunosensor.



**Figure 10.** The results study the reproducibility and stability of two series of four different electrodes of PcAb-HRP/LGG/anti-SpaA/Au-Fe<sub>3</sub>O<sub>4</sub> NPs/MGCE to determination of 10<sup>5</sup> CFU/ml bacterial suspensions from using the DPV measurements in 10mM PBS (pH7.4) containing 1.0mM H<sub>2</sub>O<sub>2</sub> and 1.0mM HQ at scan rate of 50mV/s.

Moreover, comparison between the signal current of prepared immunosensors that were stored refrigerator at 4 °C for 5, 10, and 20 days, demonstrates to decreases of 3.06%, 7.01%, and 9.10%, respectively, compared to of as synthesized immunosensor. It highlights the stability of the proposed

immunosensor. For study the reproducibility and stability of proposed immunosensor, two series of four different electrodes of PcAb-HRP/LGG/anti-SpaA/Au-Fe<sub>3</sub>O<sub>4</sub> NPs/MGCE were synthesized, and used for the determination of 10<sup>5</sup> CFU/ml bacterial suspensions from LGG through the DPV technique in 10mM PBS (pH7.4) containing 1.0mM H<sub>2</sub>O<sub>2</sub> and 1.0mM HQ at a scan rate of 50mV/s.

The practical capability of the developed immunosensor for the determination of LGG in milk and yogurt was studied and the results are summarized in Table 2. Table 2 presents that no LGG level is detected for the samples without label LGG (milk and commercial yogurt I) before the LGG spike. In contrast, the samples with label LGG (commercial yogurt II) shows the  $1.30 \times 10^4$  CFU/ml LGG before the spike of analyte. In all samples, good agreement is observed between the detected values and spiked values of LGG. The results illustrate that the components in milk and yogurt matrices do not show any influence on immunosensor detection. The obtained recovery value in the range from 101.5% to 95.0% and the RSD range from 2.57% to 4.51% indicates the acceptable precision of the developed immunosensor as a reliable electrochemical LGG sensor in food samples.

**Table 2.** The analytical determination of LGG in the prepared real samples of milk and commercial yogurts

Food samples	spiked (CFU/ml)	detected (CFU/ml)	Recovery (%)	RSD (%)
Milk	0.00	0.00	-	3.23
	$2.00 \times 10^3$	$2.02 \times 10^3$	101.00	4.08
	$2.00 \times 10^4$	$1.98 \times 10^4$	99.00	3.77
	$2.00 \times 10^5$	$2.01 \times 10^5$	100.50	4.17
Yogurt I	0.00	0.00	-	3.27
	$2.00 \times 10^3$	$2.03 \times 10^3$	101.50	2.98
	$2.00 \times 10^4$	$1.99 \times 10^4$	99.50	3.78
	$2.00 \times 10^5$	$1.96 \times 10^5$	98.00	4.51
Yogurt II	00.0	$1.30 \times 10^4$	-	3.66
	$2.00 \times 10^3$	$1.49 \times 10^4$	95.00	2.57
	$2.00 \times 10^4$	$3.29 \times 10^4$	99.50	4.18
	$2.00 \times 10^5$	$2.12 \times 10^5$	99.50	4.21

#### 4. CONCLUSION

This work presented the chemical synthesis method for preparing Au-Fe<sub>3</sub>O<sub>4</sub> NPs and the fabrication of PcAb-HRP/LGG/anti-SpaA/Au-Fe<sub>3</sub>O<sub>4</sub> NPs/MGCE as a sandwich-like immunosensor using immobilized biological molecules on the surface of Au-Fe<sub>3</sub>O<sub>4</sub> NPs. The structural analyses indicated the successful synthesis of the Au-Fe<sub>3</sub>O<sub>4</sub> NPs and the immobilization of biological molecules on the surface of Au-Fe<sub>3</sub>O<sub>4</sub> NPs. Electrochemical studies showed the high sensitivity, accuracy and selectivity, and acceptable reproducibility of developed immunosensor for the determination of LGG. Results revealed that the linear concentration of LGG is from 10 to 10<sup>9</sup> CFU/ml, and the limit of

detection was obtained at 14 CFU/ml. Results of the study on the practical capability of immunosensor for the determination of LGG in milk and yogurt illustrated that the components in milk and yogurt matrices did not show any influence on immunosensor detection, implying the developed immunosensor is a reliable electrochemical LGG sensor in food samples.

#### ACKNOWLEDGEMENT

The work was funded by the "Thirteen-five" science and technology project (JJKH20201292JY) of The Education Department of Jilin Province of China.

#### References

1. H. Maleh, M. Alizadeh, F. Karimi, M. Baghayeri, L. Fu, J. Rouhi, C. Karaman, O. Karaman and R. Boukherroub, *Chemosphere*, (2021) 132928.
2. L. Capurso, *Journal of clinical gastroenterology*, 53 (2019) S1.
3. R. Rezapour-Nasrabad, *International Journal of Pharmaceutical Research*, 11 (2019) 1.
4. S. Haddadi, R. Shahrokhirad, M.M. Ansari, S. Marzban, M. Akbari and A. Parvizi, *Anesthesiology and pain medicine*, 8 (2018) e61041.
5. A. Medghalchi, M. Akbari, Y. Alizadeh and R.S. Moghadam, *Journal of current ophthalmology*, 30 (2018) 353.
6. Y. Orooji, B. Tanhaei, A. Ayati, S.H. Tabrizi, M. Alizadeh, F.F. Bamoharram, F. Karimi, S. Salmanpour, J. Rouhi and S. Afshar, *Chemosphere*, 281 (2021) 130795.
7. J. Sun, H. Chen, Y. Qiao, G. Liu, C. Leng, Y. Zhang, X. Lv and Z. Feng, *Journal of Dairy Science*, 102 (2019) 5971.
8. Y. Yang, F. Sun, H. Chen, H. Tan, L. Yang, L. Zhang, J. Xie, J. Sun, X. Huang and Y. Huang, *Science of The Total Environment*, 758 (2021) 143631.
9. N. Derakhshan, D. Derakhshan, A. Derakhshan, G. Hashemi, M. Fallahzadeh, M. Basiratnia, Z. Bazargani, H. Jalaieian and S. Malek-Hosseini, *Saudi Journal of Kidney Diseases and Transplantation*, 22 (2011) 339.
10. S. Khosravi and S.M.M. Dezfouli, *Systematic Reviews in Pharmacy*, 11 (2020) 913.
11. S.M. Mahmoudinezhad Dezfouli and S. Khosravi, *Indian Journal of Forensic Medicine & Toxicology*, 15 (2021) 2674.
12. T. Dubois, C. Reynaert, D. Jacques, B. Lepiece and N. Zdanowicz, *Psychiatria Danubina*, 32 (2020) 158.
13. M. Khosravi, *Journal of Eating Disorders*, 8 (2020) 1.
14. X. Tang, J. Wu, W. Wu, Z. Zhang, W. Zhang, Q. Zhang, W. Zhang, X. Chen and P. Li, *Analytical chemistry*, 92 (2020) 3563.
15. Z. Yang, Y. Wei, S. Rao, L. Gao, Y. Yin, F. Xue, W. Fang, R. Gu and X. Jiao, *Journal of applied microbiology*, 121 (2016) 1406.
16. Y. Xue, D.-l. Jiang, Q. Hu, S.-q. Rao, L. Gao and Z.-q. Yang, *Food Analytical Methods*, 12 (2019) 1197.
17. Y. Gao, J. Wang, Y. Du, C. Wu, H. Li, Z. Yang, Z. Chen and Z. Yang, *Microchimica Acta*, 189 (2021) 5.
18. C. Dausset, S. Bornes, S. Miquel, N. Kondjoyan, M. Angenieux, L. Nakusi, P. Veisseire, E. Alaterre, L.G. Bermúdez-Humarán, P. Langella, E. Engel, C. Forestier and A. Nivoliez, *Scientific Reports*, 10 (2020) 17074.
19. T. Ahlroos and S. Tynkkynen, *Journal of applied microbiology*, 106 (2009)
20. A. Ito, Y. Sato, S. Kudo, S. Sato, H. Nakajima and T. Toba, *Current Microbiology*, 47 (2003) 0231.

21. M. Smith, M. McKeague and M.C. DeRosa, *MethodsX*, 6 (2019) 333.
22. W. Li, W. Jiang, S. Dai and L. Wang, *Analytical chemistry*, 88 (2016) 1578.
23. I.R. Grant, H.J. Ball and M.T. Rowe, *Applied and Environmental Microbiology*, 64 (1998) 3153.
24. Z.-Q. Shen, J.-F. Wang, Z.-G. Qiu, M. Jin, X.-W. Wang, Z.-L. Chen, J.-W. Li and F.-H. Cao, *Biosensors and Bioelectronics*, 26 (2011) 3376.
25. M. Anbarasu, M. Anandan, E. Chinnasamy, V. Gopinath and K. Balamurugan, *Spectrochimica Acta Part A: Molecular and Biomolecular Spectroscopy*, 135 (2015) 536.
26. M. Sedki, G. Zhao, S. Ma, D. Jassby and A. Mulchandani, *Sensors*, 21 (2021) 883.
27. C. Wang, J. Qian, K. Wang, X. Yang, Q. Liu, N. Hao, C. Wang, X. Dong and X. Huang, *Biosensors and Bioelectronics*, 77 (2016) 1183.
28. P. Thistlethwaite and M. Hook, *Langmuir*, 16 (2000) 4993.
29. T. Charoensuk, C. Sirisathikul, U. Boonyang, I.J. Macha, J. Santos, D. Grossin and B. Ben-Nissan, *Journal of Non-Crystalline Solids*, 452 (2016) 62.
30. L. Quaroni, I. Benmessaoud, B. Vileno, E. Horváth and L. Forró, *Molecules*, 25 (2020) 336.
31. S.M.M. Dezfouli and S. Khosravi, *European Journal of Translational Myology*, 30 (2020) 291.
32. R. Gonçalves, E.C. Pereira and L.F. Marchesi, *International Journal of Electrochemical Science*, 12 (2017) 1983.
33. S.B. Gayathri, P. Kamaraj, M. Arthanareeswari and S.D. Kala, *International Journal of Electrochemical Science*, 9 (2014) 6113.
34. J. Li, Y. Li, M. Han, X. Weng, Y. Li, Z. Lu, Q. Xu, H. Li and W. Wang, *ACS Applied Nano Materials*, 3 (2020) 9151.
35. W. Al Zoubi, J.H. Min and Y.G. Ko, *Scientific reports*, 7 (2017) 11.
36. M. Srivastava, N.R. Nirala, S.K. Srivastava and R. Prakash, *Scientific Reports*, 8 (2018) 1923.
37. M. Baghayeri, R. Ansari, M. Nodehi, I. Razavipanah and H. Veisi, *Microchimica Acta*, 185 (2018) 1.
38. Z. Guo and H. Fan, *International Journal of Electrochemical Science*, 16 (2021) 211125.
39. S.-H. Wu, X.-B. Huang, Y. Tang, L.-M. Ma, Y. Liu and J.-J. Sun, *Analytica chimica acta*, 1096 (2020) 44.
40. S. Khosravi and S.M.M. Dezfouli, *Journal of Critical Reviews*, 7 (2020) 275.
41. Y. Zhang, J. Li, Z. Wang, H. Ma, D. Wu, Q. Cheng and Q. Wei, *Scientific Reports*, 6 (2016) 23391.
42. I.-H. Cho, D.H. Kim and S. Park, *Biomaterials Research*, 24 (2020) 6.
43. B. Liu, M. Li, Y. Zhao, M. Pan, Y. Gu, W. Sheng, G. Fang and S. Wang, *Sensors*, 18 (2018) 1946.
44. J. Hajslova, T. Cajka and L. Vaclavik, *TrAC Trends in Analytical Chemistry*, 30 (2011) 204.
45. C.E. Vargas García, M. Petrova, I.J.J. Claes, I. De Boeck, T.L.A. Verhoeven, E. Dilissen, I. von Ossowski, A. Palva, D.M. Bullens, J. Vanderleyden and S. Lebeer, *Applied and environmental microbiology*, 81 (2015) 2050.
46. M. Pedrero, F.J. Manuel de Villena, M.-S. Martín, S. Campuzano, M. Garranzo-Asensio, R. Barderas and J.M. Pingarrón, *Biosensors*, 6 (2016) 56.
47. N. Ma, Z. Ma, Y. Yue and Z. Gao, *Journal of Molecular Catalysis A: Chemical*, 184 (2002) 361.
48. M.A. Delavar and P. Karimian, *Pakistan Journal of Medical & Health Sciences*, 14 (2020) 1686.